Oxygen and carbon isotope variations in Chamelea gallina shells: environmental influences and vital effects

Oxygen and carbon isotope variations in *Chamelea gallina* shells: environmental influences and vital effects

Arianna Mancuso[1,2], Ruth Yam[3], Fiorella Prada[4], Marco Stagioni[5], Stefano Goffredo[1,2*] and Aldo Shemesh[3]

[1] *Marine Science Group, Department of Biological, Geological and Environmental Sciences, University of Bologna, Bologna, Italy*

[2] *Fano Marine Center, The Inter-Institute Center for Research on Marine Biodiversity, Resources and Biotechnologies, Fano, Pesaro-Urbino Italy*

[3] *Department of Earth and Planetary Sciences, Weizmann Institute of Science, Rehovot, Israel*

4 Environmental Biophysics and Molecular Ecology Program, Department of Marine and Coastal Sciences, Rutgers, The State University of New Jersey, New Brunswick, NJ, United States

[5] *Marine Biology and Fisheries Lab, Dept. of Biological, Geological and Environmental Sciences, University of Bologna, Bologna, Italy*

***corresponding author: E-mail s.goffredo@unibo.it**

ABSTRACT

Stable isotopes in mollusc shells, together with variable growth rates and other geochemical properties, can register different environmental clues, including seawater temperature, salinity and primary productivity. However, the strict biological control over the construction of biominerals exerted by many calcifying organisms can constrain the use of these organisms for paleoenvironmental reconstructions. Biologically controlled calcification is responsible for the so called vital effects that cause a departure from isotopic equilibrium during shell formation, resulting in lower shell oxygen and carbon compared to the equilibrium value. We investigated shell oxygen and carbon isotopic composition of the bivalve *Chamelea gallina* in six sites along a latitudinal gradient on the Adriatic Sea (NE Mediterranean Sea). Seawater $\delta^{18}O$ and $\delta^{13}C_{DIC}$ varied from North to South, reflecting variations in seawater temperature, salinity, and chlorophyll concentration among sites. Shell $\delta^{18}O$ and $\delta^{13}C$ differed among sites and exhibited a wide range of values along the ~400 km latitudinal gradient, away from isotopic equilibrium for both isotopes. These results hampered the utilization of this bivalve as a proxy for environmental reconstructions, in spite of *C. gallina* showing promise as a warm temperature proxy. Rigorous calibration studies with a precise insight of environment and shell growth are crucial prior to considering this bivalve as a reliable paleoclimatic archive.

Keywords: bivalve; shell stable isotopes; Adriatic Sea; latitudinal gradient; vital effect

1 INTRODUCTION

Marine calcifying organisms can be considered valuable recorders of past environmental change in marine habitats (Rhoads & Lutz, 1980; Bemis *et al.*, 1998; Chauvaud *et al.*, 2005; Jones *et al.*, 2009; Schöne & Gillikin, 2013; Vihtakari *et al.*, 2017). In particular, mollusc shells are potential paleo-environmental archives due to their seasonal deposition of carbonate material, retaining high resolution temporal records of the ambient physical and chemical conditions during growth that can be detected by shell oxygen and carbon isotope composition (Klein *et al.*, 1996a; Schöne *et al.*, 2003; Purroy *et al.*, 2018).

In molluscs, calcification occurs within the extrapallial fluid (EPF), which is secreted by the mantle and is isolated from seawater (Wheeler, 1992). The composition of the EPF might be significantly altered with respect to seawater due to the influence of mantle metabolic activity or to the contribution of carbon from metabolic sources (Tanaka *et al.*, 1986; Klein *et al.*, 1996b). As a consequence of such processes, termed "vital effects" and classified as kinetic or metabolic isotope effects, biomineral compositions may depart from isotopic equilibrium. (McConnaughey, 1989a, 1989b). Thus, developmental or ontogenetic changes can obscure environmental signals, such as oxygen and carbon isotopic equilibrium fractionation, that occur in some species (McConnaughey, 1989a; Gillikin *et al.*, 2007; Schöne, 2008). Furthermore, shell growth relies on various environmental factors, including temperature, salinity and food availability, that are responsible for varying biomineralization rates and shell growth cessation when beyond the environmental optimum of the organism (Schöne, 2008; Leng & Lewis, 2016). Therefore, a detailed understanding of the physiology and growth rates of the organism that produces the mineralized structures is crucial to obtaining a reliable reading of geochemical signals from mollusc shells.

Oxygen ($\delta^{18}O$ derived from $^{18}O/^{16}O$ ratios) and carbon ($\delta^{13}C$ derived from $^{13}C/^{12}C$ ratios) isotopic composition of marine mollusc carbonates are robust proxies for seawater

69 temperature and dissolved inorganic carbon, respectively (Krantz *et al.*, 1987; Bemis & Geary,
70 1996; Hickson *et al.*, 1999; Goodwin *et al.*, 2001; Elliot *et al.*, 2003). Shell oxygen isotope
71 composition ($\delta^{18}O_{shell}$) is a function of temperature, salinity and the oxygen isotope composition
72 of seawater ($\delta^{18}O_{sw}$) at the time of precipitation (Epstein & Mayeda, 1953; Craig, 1965). The
73 temperature dependence of $\delta^{18}O$ fractionation in biogenic carbonates has been linked to
74 species-specific vital effects (Wefer & Berger, 1991; Bemis *et al.*, 1998; Böhm *et al.*, 2000). Shell
75 carbon isotope composition ($\delta^{13}C_{shell}$) is determined by the isotopic composition of the
76 dissolved inorganic carbon in seawater ($\delta^{13}C_{DIC}$) and by the proportion of metabolic carbon
77 involved in the calcite/aragonite precipitation (Sadler *et al.*, 2012). The amount of metabolic
78 respiratory CO_2 incorporated into the skeleton is species-dependent, varying from less than
79 10% to over 35%, and it can be high enough to overshadow the $\delta^{13}C_{DIC}$ signal (Klein *et al.*,
80 1996b; Lorrain *et al.*, 2004; Gillikin *et al.*, 2005, 2006).

81 While the incorporation of respired CO_2 within the body of an organism is linked to
82 metabolic effects (McConnaughey *et al.*, 1997), kinetic effects are specifically associated with
83 processes such as shell crystal growth rate, hydration and hydroxylation of CO_2 in solution
84 (McConnaughey, 1989b) and the isotope fractionation between species of $\delta^{13}C_{DIC}$ which are
85 present in the calcifying fluids (Spero *et al.*, 1997; Zeebe, 1999; Adkins *et al.*, 2003; Tripati *et*
86 *al.*, 2010). Taking into account the amplitude of the biologically induced fractionation, in
87 addition to environmental conditions, is crucial for a reliable interpretation of $\delta^{18}O$ and $\delta^{13}C$
88 signatures from molluscs specimens.

89 The present study aimed to investigate shell $\delta^{18}O$ and $\delta^{13}C$ in the clam *Chamelea gallina*
90 along a latitudinal gradient in the Adriatic Sea (~400km). Shell isotopic profiles of *C. gallina*
91 were also investigated to study ontogenetic variations in shell $\delta^{18}O$ and $\delta^{13}C$ along the gradient.
92 This study also monitored seawater $\delta^{18}O$ and $\delta^{13}C_{DIC}$ along the Adriatic Sea latitudinal gradient,
93 where the presence of Po river delta plays a crucial role in the biogeochemical processes of this

basin. The Po is the largest Italian river in terms of both length (652 km long) and average discharge (1,500 m^3 s^{-1}; Montanari, 2012), supplying over 50% of freshwater input to the Northern Adriatic basin (Degobbis *et al.*, 1986) and about 20% of total river discharge in the Mediterranean Sea (Russo & Artegiani, 1996). Fluvial $\delta^{13}C_{DIC}$ has usually lower isotopic composition than oceanic due to the presence of CO_2 originated from the decomposition of terrestrial vegetation (McConnaughey & Gillikin, 2008). In the Po Plain-Adriatic Sea system, a strong geomorphological change took place during the Holocene in response to the glacio-eustatic sea-level variations (Amorosi *et al.*, 2019). In the past, the North Western Adriatic coastal area was characterized by estuary systems, bounded seaward by a series of sandbars that isolated coastal lagoons and limited riverine plumes into the Adriatic (Amorosi *et al.*, 2019). This past more stable shoreface depositional setting due to reduced influence of riverine plumes, warmer temperature and higher aragonite saturation state than today seemed to reduce the thermodynamic work required for organisms to deposit calcium carbonate (Hall-Spencer & Harvey, 2019), making the calcification less expensive in terms of metabolic cost (Clarke, 1993; Cheli *et al.*, 2021). Nowadays, the western Adriatic basin is characterized by the northern area with shallow continental shelf, representing the result of several southward progradations driven by sea level cycles, by the central Adriatic Sea, a small remnant basin reaching 260 m water depth and confined to the north by the Po River delta formed during the last sea level lowstand and by the Southern Adriatic Sea, originated as a consequence of the interaction between mass transport processes and deep water circulation (Ridente *et al.*, 2007, 2008). The Adriatic Sea is a dynamic environment influenced by terrestrial, atmospheric and oceanic processes that provide many challenges to understanding these systems (Canuel *et al.*, 2012; Pérez *et al.*, 2016). In addition to environmental drivers such as freshwater discharge and coastal upwelling, it can be impacted, as the other coastal zones, by increases in atmospheric pCO_2 with the alteration of the distribution of reactive inorganic carbon species,

thus reducing pH values and the saturation state for calcium carbonate minerals (Ω) (Feely *et al.*, 2004; Gazeau *et al.*, 2007; Harris *et al.*, 2013; Pérez *et al.*, 2016) and anthropogenic change of river basins that further influence the natural export of water, nutrients, and carbon to estuarine and coastal marine ecosystems (Regnier *et al.*, 2013; Pérez *et al.*, 2016). The carbonate chemistry of riverine-influenced near shore environments is therefore affected by lower salinity and resultant decreased alkalinity, eutrophication and resultant production/respiration cycles (Salisbury *et al.*, 2008; Pérez *et al.*, 2016).

This study covers several sites along the latitudinal gradient in the Adriatic Sea and will contribute to the understanding whether vital/ontogenic process or environmental conditions govern the shell isotopic signature in the bivalve *C. gallina*, giving insight into the use of bivalve archives as providers of environmental information.

2 MATERIALS AND METHODS

2.1 Sample collection and treatment

Specimens of *C. gallina* were collected from six sites in the Western Adriatic Sea from 45°42′N to 41°55′N, spanning ~400 km of latitudinal gradient, ~2°C of average sea surface temperature, ~9 PSU of average sea surface salinity and ~5 mg/m^3 of average chlorophyll concentration (Fig. 1-2). Because of the shallow sampling conditions (not beyond 5 meters of water depth) and the well mixed water column we assume homogeneous environmental parameters between surface and bottom.

Clams were sampled using hydraulic dredges at 3–5 m depth on sandy or mud bottoms along the Eastern Italian coasts in six sites from North to South (Fig. 1), Monfalcone (MO), Chioggia (CH), Goro (GO), Cesenatico (CE), San Benedetto (SB) and Capoiale (CA). Seawater

144 samples were collected in the six sites in summer (August) and winter (February) in duplicate.
145 In August and February, seawater was the warmest and coldest of the year, respectively, with
146 no sharp shifts in salinity, as occurred during autumn and spring in response to increases
147 rainfall and corresponding river discharge. Although two seawater samples did not allow the
148 capture of seasonal variability over months and years, they can indicate annual seawater
149 isotopes extremes. Seawater samples were stored in plastic jars of 100 ml without additional
150 treatments for $\delta^{18}O$ and in glass bottles with 1 ml of saturated mercuric chloride ($HgCl_2$) for
151 $\delta^{13}C_{DIC}$, in order to stop all biological activity.
152
153 **2.2 Oxygen and carbon isotopic compositions**
154 For shell $\delta^{18}O$ and $\delta^{13}C$ analysis, 7-8 shells from each site were selected and treated with a
155 solution of H_2O_2 (10% buffered with ammonium hydroxide) to clean the surface from
156 exogenous sources of oxygen and carbon. Shell powders were manually collected by means of
157 a dental drill (0.5 mm diameter) on the shell surface. The isotope ratios of the shells were
158 determined by using "average shell powder", which is the combined powders drilled in several
159 points along the shell growth axis (Fig. S1). Seasonal $\delta^{18}O$ and $\delta^{13}C$ profiles were carried out on
160 one shell from each of the five sites, by drilling "spot" samples in sequence from the umbo
161 (oldest zone of the shell) to the ventral edge (youngest zone) along the shell growth axis with
162 ~1.4 mm mean spatial resolution. The necessity of roasting to pyrolise the organic matter
163 before isotopes analyses (350°C for 45 min in vacuo; Keller *et al.*, 2002) was tested by analyzing
164 12 random powder samples taken from all sites. Shell $CaCO_3$ samples of 180-250 µg of powder
165 were flushed with helium gas and reacted with 100% orthophosphoric acid (H_3PO_4) and left to
166 equilibrate at 25°C for 24h. The evolved CO_2 gas was analyzed using a Finnigan GasBench II
167 connected in line to a Finnigan MAT252 isotope ratio mass spectrometer at the Department of
168 Earth and Planetary Sciences, Weizmann Institute of Science. The shell $\delta^{18}O$ and $\delta^{13}C$ data are

reported against VPDB-standard.

The analysis of seawater oxygen isotope ($\delta^{18}O_{sw}$) was performed by mixing 0.5 ml of seawater with 0.5% CO_2 in helium at 25°C for 24h. The values are reported in per-mill relative to the Vienna Standard Mean Ocean Water (VSMOW; ±0.05‰ long-term precision of laboratory). For carbon isotopes analysis of seawater ($\delta^{13}C_{DIC}$), 1 ml of seawater was injected into gas vials pre-flushed with helium and left to react with 0.15 ml H_3PO_4 at 25°C for 24h. The results are reported relative to the international Vienna-PeeDee Belemnite standard (VPDB; ±0.08‰ long-term precision of $NaHCO_3$ laboratory standard).

SST in each site were reconstructed from shell isotopic composition along the growth axis and $\delta^{18}O_{sw}$ to compare with SST data from satellite, by using the equation from Grossman & Ku, 1986 [$T = 20.6 - 4.34(\delta^{18}O_{arag} - (\delta^{18}O_{sw} - 0.27))$] (Bemis *et al.*, 1998). In particular, SST were estimated from seasonal $\delta^{18}O_{shell}$ profile corrected with measured $\delta^{18}O_{sw}$ (winter, summer and average values for each sites) and with calculated $\delta^{18}O_{sw}$ reconstructed from salinity data (winter, summer and average sea surface salinity for each sites), using the equation derived from Purroy *et al.*, 2018 for the coastal areas in the eastern Adriatic Sea [$\delta^{18}O_{sw} = 0.23$ x salinity - 7.54]. The estimated SSTs were temporally aligned with satellite data, starting from the shell ventral margin corresponding to time of sampling, and backwards sinusoidal sequence of $\delta^{18}O_{shell}$ defined the seasonal values to consider in the equations (winter for higher peaks, summer for lower peaks and average values for intermediate points).

2.3 Diffractometric measurements

XRD analyses were carried out in one specimen for each site to determine shell mineral phases. Diffraction patterns were obtained by means of a D2 Phaser diffractometer with Lynxeye detector, using Cu-Kα radiation generated at 30 kV and 10 mA at the department of Earth and Planetary Sciences in Weizmann Institute of Science. XRD patterns were analyzed using the

194 Diffract.Eva software.

195

196 **2.4 Shell growth parameters**

197 Clam shell length (L, maximum length on the anterior-posterior axis), was calculated with
198 ImageJ software after capturing shell shape with a scanner. Annual growth rates were
199 calculated with the length/age ratio, by using the age obtained from $\delta^{18}O$ profile along the shell
200 growth axis.

201

202 **2.5 Environmental parameters**

203 For each site, sea surface temperature (SST; °C) and sea surface salinity (SSS; PSU) data were
204 extrapolated from the database of the Euro-Mediterranean Center on Climate Change. The
205 annual average of SST and SSS were obtained from daily values from July 2011 to July 2015,
206 while chlorophyll concentration (CHL; mg/m^3) was calculated from monthly values from the
207 *GlobColour data* by ACRI-ST, France. The selected range of four years for the environmental
208 parameters ensured to enclose the full lifespan of *C. gallina*, reported to be of two-three years
209 in the Adriatic Sea (Mancuso *et al.*, 2019).

210

211 **2.6 Statistical analyses**

212 Significant differences of SST, SSS, CHL, $\delta^{18}O_{sw}$, $\delta^{13}C_{DIC}$ and shell $\delta^{18}O$ and $\delta^{13}C$ among sites were
213 tested with the one-way analysis of variance (ANOVA). The non-parametric Kruskal-Wallis
214 rank test was used when assumptions for parametric statistics were not fulfilled. The
215 correlations between $\delta^{18}O_{sw}$ and $\delta^{13}C_{DIC}$ with latitude were calculated with Spearman's rank
216 correlation coefficient (r_S). A General Additive Model (GAM; package mgcv) was used to analyze
217 the influence of different environmental factors on shell $\delta^{18}O$ and $\delta^{13}C$ data. GAM are non-
218 parametric regression techniques that are not restricted by linear relationships, thus they

provide a flexible method for analysis when the relationship between variables is complex. GAM was selected based on the gain in deviance explained (%) and on the reduction in Akaike's information criterion (AIC) and generalized cross validation score (GCV) compared to linear model (Table S1). All data analyses were computed using RStudio Software(RStudio Team, 2020).

3 RESULTS

3.1 Environmental parameters, $\delta^{18}O_{sw}$ and $\delta^{13}C_{DIC}$

SST, SSS and CHL from satellite were significantly different among sites in the Adriatic Sea (Kruskal-Wallis test, $p<0.001$; Fig. 1-2). SST and SSS correlated negatively with latitude, while CHL showed the opposite trend.

Summer, winter and annual mean $\delta^{18}O_{sw}$ and $\delta^{13}C_{DIC}$ were significantly different among sites (Kruskal-Wallis test, $p<0.001$, Table 1) and correlated negatively with latitude, except for $\delta^{13}C_{DIC}$ in summer (Fig. 3). $\delta^{18}O_{sw}$ showed positive values while in Chioggia and Goro the $\delta^{18}O_{sw}$ shifted sharply towards negative values in summer (-1.24‰ and -2.84‰, respectively), even lower than the values in winter (Table 1; Fig 3). In winter, negative $\delta^{18}O_{sw}$ values were still found in Goro (-0.65‰), together with Cesenatico (-0.60‰) and the resulting annual mean $\delta^{18}O_{sw}$ showed considerably lower values in Goro (-1.75‰) and marginally lower in Chioggia and Cesenatico (-0.19‰ and -0.06‰, respectively; Table 1; Fig 3). Goro stood out for its deeply low values of $\delta^{13}C_{DIC}$ in both seasons (-3.54‰ in summer and -2.34‰ in winter), while Capoiale was the only site with positive value of $\delta^{13}C_{DIC}$, both in summer and winter season (0.28‰ and 0.11‰, respectively; Table 1; Fig 3).

Using the annual mean temperature from all sites along the latitudinal gradient (17.25°C), the estimated isotopic value for biological aragonite deposited in equilibrium with ambient seawater {calculated from Grossman and Ku, 1986 for oxygen [$T = 20.6 - 4.34(\delta^{18}O_{arag} - (\delta^{18}O_{sw} - 0.27))$] and Romanek et al., 1992 for carbon ($\delta^{13}C_{arag} = \delta^{13}C_{DIC} + 2.7$)}, resulted in 0.77‰ +/- 0.25‰ for $\delta^{18}O$ and 2.70‰ for $\delta^{13}C$ (Fig. 4). $\delta^{18}O_{sw}$ and $\delta^{13}C_{DIC}$ were not included in the equation as the graph axis are, $\delta^{18}O_{shell} - \delta^{18}O_{sw}$ and $\delta^{13}C_{shell} - \delta^{13}C_{DIC}$, respectively.

3.2 Shell $\delta^{18}O$ and $\delta^{13}C$

$CaCO_3$ of the analyzed shells of *C. gallina* consisted of aragonite as indicated by XRD patterns obtained for six specimens (one specimen per site; Fig. 5). The roasting test showed no differences in the $\delta^{18}O_{shell}$ and $\delta^{13}C_{shell}$ between roasted and not roasted powders, with a homogeneous distribution of values obtained from the two procedures ($p>0.05$; Supplementary Fig. S2). Hence, additional roasting treatment was avoided.

$\delta^{18}O_{shell}$ and $\delta^{13}C_{shell}$ were different among sites (Kruskal-Wallis test, $p<0.001$; Table 2). In order to consider the isotopic composition of the local seawater, shell isotope data were corrected with annual mean $\delta^{18}O_{sw}$ and $\delta^{13}C_{DIC}$ of each site and the corrected data (indicated as $\delta^{18}O_{shell} - \delta^{18}O_{sw}$ and $\delta^{13}C_{shell} - \delta^{13}C_{DIC}$) were still different among sites (Kruskal-Wallis test, $p<0.001$; Table 2). A strong positive correlation between $\delta^{18}O_{shell} - \delta^{18}O_{sw}$ and $\delta^{13}C_{shell} - \delta^{13}C_{DIC}$ was observed considering the entire isotope dataset ($p<0.001$; Fig. 4). The measured isotopic values were far from the mean annual estimated aragonite equilibrium value (0.77‰; Fig. 4). Only Goro, clustered away from the other sites for both $\delta^{18}O_{shell} - \delta^{18}O_{sw}$ and $\delta^{13}C_{shell} - \delta^{13}C_{DIC}$, showing $\delta^{18}O_{shell} - \delta^{18}O_{sw}$ values close to the aragonite equilibrium value (Fig. 4). Moreover, only Goro showed positive $\delta^{18}O_{shell} - \delta^{18}O_{sw}$ values, while San Benedetto and Capoiale, the warmer sites, showed lower values (Table 2; Fig. 4). $\delta^{18}O_{shell} - \delta^{18}O_{sw}$ showed a slight positive correlation with latitude ($p<0.05$; Table S2; Fig. 6), due to higher values reported at Goro (0.76‰), while

268 the two Northern sites, Monfalcone and Chioggia, had lower values (Table 2; Fig. 6). $\delta^{18}O_{shell}$ -
269 $\delta^{18}O_{sw}$ was also correlated with SST and SSS ($p<0.001$; Table S2; Fig. 6) and with chlorophyll
270 ($p<0.05$; Table S2; Fig. 6).

271 $\delta^{13}C_{shell}$ - $\delta^{13}C_{DIC}$ showed no correlation with latitude (Table S2), despite the similar
272 pattern of $\delta^{18}O_{shell}$ - $\delta^{18}O_{sw}$, with Goro that presented the highest values (Table 2-S2). SST, SSS
273 and CHL showed significant correlations with shell $\delta^{13}C_{shell}$ - $\delta^{13}C_{DIC}$ among the six sites ($p<0.01$
274 for SST and $p<0.001$ for SSS and CHL; Table S2; Fig. 6).

275 Seasonal analysis obtained from the drilled spots along a single shell growth axis
276 revealed that the drilling method, with a mean spatial resolution of ~1.4 mm, resulted in a
277 sinusoidal sequence of lighter and heavier $\delta^{18}O_{shell}$ with the detection of distinctive seasonal
278 peaks in the $\delta^{18}O_{shell}$ - $\delta^{18}O_{sw}$ (Fig. 7). The age of five specimens could be defined by counting
279 the sequence of summers (lighter values) and winters (heavier values), and the reduction of
280 the growth rates could be detected with increasing age by the reduction of width of sinusoidal
281 sequences (Fig. 7). The shells from Monfalcone and Goro were probably born at the end of
282 summer, while the shells from the other sites were born early in spring or at the beginning of
283 summer, according with the first $\delta^{18}O_{shell}$ values in each curve (Fig. 7).

284 SST derived from measured $\delta^{18}O_{shell}$ and $\delta^{18}O_{sw}$ reflected the SST from satellite during
285 warm seasons in all sites except in Goro, where only SST calculated with $\delta^{18}O_{sw}$ predicted from
286 summer salinity data aligned with summer SST from satellite (Fig. 8). In the cold season SST
287 derived from both measured $\delta^{18}O_{sw}$ and predicted $\delta^{18}O_{sw}$ from salinity seemed to overestimate
288 the temperature in all sites (Fig. 8). In Goro, reconstructed SST from $\delta^{18}O_{sw}$ results are
289 inconsistent with winter seasonal peaks (Fig. 8). In general, the two methods used for obtaining
290 SST from measured $\delta^{18}O_{sw}$ and from predicted $\delta^{18}O_{sw}$ from salinity agree, showing similar SST
291 in five sites, except in Goro (Fig. 8). In Goro, SST derived from measured $\delta^{18}O_{sw}$ showed no

seasonal profile, suggesting an apparent uncertainty in the measured $\delta^{18}O_{sw}$ values in this site (Fig. 8).

$\delta^{13}C_{shell}$ - $\delta^{13}C_{DIC}$ of *C. gallina* differed within the shells and among sites, showing a decreasing trend from the umbo to the ventral edge in all shells and higher variability for $\delta^{13}C_{shell}$ - $\delta^{13}C_{DIC}$ in the shells from the Northern sites (Fig. 7). The large variability in $\delta^{13}C_{shell}$ - $\delta^{13}C_{DIC}$ was observed especially over 30 mm in the shells of Goro and Cesenatico, where considerable peaks of reduced $\delta^{13}C_{shell}$ - $\delta^{13}C_{DIC}$ were depicted (-4.17‰ and -3.91‰ respectively; Fig. 7). Positive correlation was found between shell carbon isotope values and annual growth rate (Fig. 9).

4 DISCUSSION

Shell $\delta^{18}O$ and $\delta^{13}C$ of the clam *C. gallina* and seawater oxygen and carbon isotope signatures were investigated for the first time under varying temperature, salinity, and chlorophyll concentration conditions along a wide latitudinal gradient in the Adriatic Sea. The Po river inflows in the Northern Adriatic Sea and heavily modifies salinity and chlorophyll concentrations from North to South (Gilmartin *et al.*, 1990; Catalano *et al.*, 2014). Po river is responsible for 50% of the total nutrient input (Pettine *et al.*, 1998), that gives rise to phytoplankton blooms in spring, making the Northern Adriatic Sea the area with the highest average primary production in the Adriatic basin (588g C m^2 y^1; Gilmartin *et al.*, 1990). In contrast, in the Middle and Southern Adriatic Sea primary production is significantly lower (137 and 97g C m^2 y^1, respectively), resulting in a relevant eutrophic/oligotrophic gradient along the Eastern coasts of Italy from North to South (Giordani *et al.*, 2002).

316 The biology of the clam *C. gallina* in the Adriatic Sea was already studied in terms of growth
317 rate (Keller *et al.*, 2002; Mancuso *et al.*, 2019; Bargione *et al.*, 2020), physiology (Matozzo *et al.*,
318 2007; Monari *et al.*, 2007a, 2007b), and shell properties (Gizzi *et al.*, 2016; Mancuso *et al.*, 2019;
319 Cheli *et al.*, 2021). A previous study conducted in the Bay of Trieste in the North of the Adriatic
320 Sea investigated the shell isotopic composition of *C. gallina* in relation to its growth rates and
321 settlement time (Keller *et al.*, 2002). However, this confined area is not representative of the
322 wide shifts in *C. gallina* habitat from North to South of the Adriatic basin that influence shell
323 growth (Mancuso *et al.*, 2019).
324
325 **4.1 $\delta^{18}O_{sw}$ and $\delta^{13}C_{DIC}$**
326 In this study, both $\delta^{18}O_{sw}$ and $\delta^{13}C_{DIC}$ varied along the ~400 km transect in the Adriatic Sea. The
327 annual $\delta^{18}O_{sw}$ varied by 3.27‰ VSMOW along the latitudinal gradient, in contrast to the
328 remarkably constant $\delta^{18}O_{sw}$ along the 850 km North-South transect in the Italian Western coast
329 (0.65‰ ± 0.23 SD; Prada *et al.*, 2019). The main driver controlling $\delta^{18}O_{sw}$ in this region is the
330 increase of freshwater inflows and the large salinity changes, from ca. 29 to 37 PSU, from the
331 area around the Po delta towards the South. Freshwater mixing from the Po river ($\delta^{18}O$ close
332 to -10‰; Bortolami *et al.*, 1973) leads to low salinity conditions (< 30 PSU) and extremely low
333 $\delta^{18}O_{sw}$ values (-1.75‰) in Goro. The Po is dominated by two annual floods due to raised rainfall
334 in autumn and snow-melt in spring (Flora & Longinelli, 1989; Tesi *et al.*, 2007) and largest
335 minimum, largest average and largest maximum daily river flow are observed to be 275 $m^3 s^{-1}$,
336 1470 $m^3 s^{-1}$ and 10 300 $m^3 s^{-1}$, respectively (Montanari, 2012). The freshwater gain along the
337 coastline of the Northern basins results in a negative difference between the freshwater losses
338 by evaporation and the gains by runoff and precipitation, making the Adriatic Sea a dilution
339 basin compared to the Mediterranean Sea as a whole (Raicich, 1996). Moreover, the surface
340 circulation of the Adriatic Sea is primarily thermohaline, driven by dense water formation

related to the surface heat losses: cool and with low salinity North Adriatic dense Deep Water (NAdDW), that flows southwards and Southern Adriatic dense Deep Water (SAdDW), favoured by cyclonic gyre (Russo & Artegiani, 1996; Zavatarelli *et al.*, 1998). Positive $\delta^{18}O_{sw}$ values were reported in the Southern sites (1.52‰ in Capoiale), likely due to the supply of saltier and isotopically heavier seawater from the Southern Adriatic, such as the Levantine Intermediate Water (LIW) that flows northwards in the Adriatic through the Otranto Strait (Stenni *et al.*, 1995). $\delta^{13}C_{DIC}$ values also strongly varied along the latitudinal gradient with a range of 3.14‰, compared to the Eastern and Western Mediterranean $\delta^{13}C_{DIC}$ values, 0.41‰ and 0.43‰, respectively (Pierre, 1999). $\delta^{13}C_{DIC}$ increased from North (-0.98‰ in Monfalcone) to South (0.20‰ in Capoiale) with a sharp depleted value in the Po delta area (-2.94‰ in Goro). $\delta^{13}C_{DIC}$ along the gradient reflected the contribution of isotopically light carbon from freshwater inflow ($\delta^{13}C_{DIC}$ close to -10.5‰ ± 0.4; Marchina, 2015), from sites around the Po delta.

4.2 Shell $\delta^{18}O$

Along the latitudinal gradient, temperature and salinity covary and their decrease towards Northern sites led to an $\delta^{18}O_{shell}$ - $\delta^{18}O_{sw}$ increase. Indeed, at thermodynamic equilibrium, $\delta^{18}O_{shell}$ depends on the precipitation temperature and seawater $\delta^{18}O$ (Epstein *et al.*, 1951; Craig, 1965; Grossman & Ku, 1986). $\delta^{18}O_{shell}$ - $\delta^{18}O_{sw}$ also reflected differences in $\delta^{18}O$ ranging from 0.76‰ in Goro to -1.28‰ in Capoiale. While the site of Goro was close to the expected oxygen isotopic equilibrium (0.77‰), the other five sites showed a negative offset from equilibrium, with the largest offset in Capoiale (-2.05‰). The $\delta^{18}O_{shell}$ - $\delta^{18}O_{sw}$ fluctuation of 2.04‰ between Goro and Capoiale would require temperature variations of about 9°C (Craig, 1965; Grossman & Ku, 1986) if temperatures were the only cause of the $\delta^{18}O_{shell}$ - $\delta^{18}O_{sw}$ fluctuation. $\delta^{18}O$ values are also changeable in relation to salinity of the habitat (Craig, 1965) and high fluctuations of salinity in Goro, the site close to Po delta, were likely responsible for

366 the deviation of temperature derived from measured $\delta^{18}O_{shell}$ - $\delta^{18}O_{sw}$, that didn't reflect the
367 annual fluctuation of seawater temperature. The two Northern sites, Monfalcone and Chioggia,
368 had lower values of $\delta^{18}O_{shell}$ - $\delta^{18}O_{sw}$, suggesting a minor influence of Po freshwater mixing and
369 a contribution of heavier $\delta^{18}O_{sw}$ from the Eastern Adriatic coast.

370 Temperatures reconstructed from $\delta^{18}O_{shell}$ - $\delta^{18}O_{sw}$ showed that higher SST agreed well
371 with real summer SST, while lower SST was consistently higher than the real winter SST
372 obtained from satellite data. This inconsistency could be attributed to the fact that *C. gallina*
373 precipitates the shell carbonate preferentially during the warm period, while considerably
374 reducing its activity during the cold season (Cespuglio *et al.*, 1999; Keller *et al.*, 2002). The same
375 seasonality of shell growth in the Adriatic Sea was found in the long-lived bivalve *Glycymeris*
376 *pilosa* and in the venerid *Callista chione* and *Venus verrucosa*, that showed to be a promising
377 archive for the reconstruction of summer seawater temperatures with the slowest growth
378 during winter (Purroy *et al.*, 2018; Peharda *et al.*, 2019; Uvanović *et al.*, 2021). Shell deposition
379 with warm temperatures was reported also for other bivalves from different parts of the globe,
380 such as *Mercenaria stimpsoni*, *Chione cortezi* and *Phacosoma japonicum*, showing that these
381 shells cannot be used as archives of winter temperatures (Tanabe & Oba, 1988; Goodwin *et al.*,
382 2001; Kubota *et al.*, 2017). In agreement with these previous results, *C. gallina* might be a warm
383 season temperature proxy, suggesting additional complexity in utilizing *C. gallina* shells in
384 paleoclimate studies. Indeed, when shell growth rate is not constant during the year, growth
385 suspensions hamper bivalves from providing uninterrupted records of environmental
386 conditions (Goodwin *et al.*, 2003).

387 It has been suggested that kinetic effects , associated with the hydration reaction and
388 carbonate biomineralization, during higher calcifications rates increase the relative amount of
389 ^{16}O incorporated in the newly formed shell, resulting in more negative $\delta^{18}O_{shell}$ signatures than
390 equilibrium values (McConnaughey, 1989a). The shells of Southern sites (with higher growth

391 rates; Mancuso *et al.*, 2019), showed the larger oxygen isotopic offset from expected
392 equilibrium, suggesting that together with temperature and salinity, kinetic effects could also
393 explain this observed departure. As bivalves mostly use the oxygen of the ambient water (HCO_3^-
394) rather than ingested food for shell growth (Epstein & Mayeda, 1953; McConnaughey, 1989a),
395 metabolic isotope effects related to respiration can be excluded.

396 From $\delta^{18}O_{shell}$ - $\delta^{18}O_{sw}$ profiles along the *C. gallina* growth direction we could derive
397 considerations on growth rates at the investigated sites in the Adriatic Sea. $\delta^{18}O_{shell}$ - $\delta^{18}O_{sw}$
398 profiles indicated that samples of Cesenatico, San Benedetto and Capoiale were born in spring,
399 while the samples of Monfalcone and Goro, with colder water, were born later in summer. A
400 notable reduction in growth rates with increasing length was also observed in the decreasing
401 amplitude of sinusoidal sequence with clam size. By counting age from seasonal $\delta^{18}O_{shell}$ - $\delta^{18}O_{sw}$
402 peaks, *C. gallina* reached a length of about 20 mm after 1 year in the Southern sites (San
403 Benedetto and Capoiale), and about 13 mm after 1 year in the Northern site (Monfalcone),
404 indicating higher linear extension rates towards the South, in agreement with the previous
405 study (Mancuso *et al.*, 2019).

406

407 **4.3 Shell $\delta^{13}C$**

408 $\delta^{13}C_{shell}$ - $\delta^{13}C_{DIC}$ exhibited a ~1.5‰ range with the largest difference between Goro (0.80‰)
409 and San Benedetto sites (-0.69‰). Seawater $\delta^{13}C_{DIC}$ and metabolic carbon from bivalve
410 respiration and diet significantly affect shell $\delta^{13}C$ values (McConnaughey, 1989b, 1989a;
411 Lorrain *et al.*, 2004; Gillikin *et al.*, 2006). In this study, $\delta^{13}C_{shell}$ - $\delta^{13}C_{DIC}$ was not correlated with
412 latitude, unlike $\delta^{13}C_{DIC}$, implying the contribution of metabolic carbon in *C. gallina* shells.
413 Molluscs shells in coastal areas incorporate carbon from both the riverine and marine
414 reservoirs, so $\delta^{13}C_{shell}$ reflects the mixture (Mook & Vogel, 1968; Gillikin *et al.*, 2006). In this
415 study, the $\delta^{13}C_{shell}$ - $\delta^{13}C_{DIC}$ of *C. gallina* increased with decreasing salinity and increasing

chlorophyll concentration, perhaps as a result of decreasing calcification. *C. gallina* shows reduced calcification rate with increasing chlorophyll concentration along the same gradient, perhaps as a result of increased sedimentation as a result of river discharges in proximity to the Po delta, which could negatively impact the feeding mechanisms of the clams (McConnaughey & Gillikin, 2008; Pérez *et al.*, 2016; Mancuso *et al.*, 2019).

$\delta^{13}C_{shell}$ - $\delta^{13}C_{DIC}$ profiles along the growth axis showed lower values with increasing length, more pronounced in the Northern sites, with Goro showing the larger ontogenetic variability (up to 4.8‰) between the umbo (the older part of shells) and the ventral margin (the youngest part of shells). In previous studies, the general decreasing trend of $\delta^{13}C$ through ontogeny was observed to be either caused by the influence of pore water $\delta^{13}C_{DIC}$ gradients, or effects of metabolic changes (Krantz *et al.*, 1987; Elliot *et al.*, 2003; Lorrain *et al.*, 2004; Gillikin *et al.*, 2007). Indeed, a deeper position in the sediment of older specimens seemed to lead to an increased supply of ^{13}C depleted pore water produced by the oxidation of organic matter or to the incorporation of larger amounts of respiratory CO_2 (Keller *et al.*, 2002; Lorrain *et al.*, 2004; McConnaughey & Gillikin, 2008). Infaunal bivalves may show isotopically depleted values compared to epifaunal species (Krantz *et al.*, 1987; Keller *et al.*, 2002). Another possible explanation could be the variation of the metabolism associated with shell growth rates. Rosenberg and Hughes, 1991 found lower mantle metabolic activity in faster growing shell portions in *Mytilus edulis*. Lorrain et al., 2004 reported a reduction in the $\delta^{13}C_{shell}$ of *Pecten maximus* as result of increasing utilization of ^{13}C depleted respiratory CO_2 through ontogeny. Similarly, higher metabolic rates needed to support carbon requirements for calcification could explain the decrease of $\delta^{13}C_{shell}$ - $\delta^{13}C_{DIC}$ through ontogeny observed in *C. gallina*. The strong link between carbon isotopes and bivalve metabolic activity suggests that carbon isotopes are not reliable indicators of environmental conditions in biogenic carbonates given the high

variability of metabolic carbon across seasons, shell growth rates and ontogenetic variations (Lorrain *et al.*, 2004; Geist *et al.*, 2005; Gillikin *et al.*, 2006).

Chamelea gallina showed a negative offset of 1.9‰ in Goro and 3.4‰ in San Benedetto from the expected carbon isotopic equilibrium (2.7‰), in agreement with most benthic species that generally have depleted $\delta^{13}C$ values compared to carbon isotopic equilibrium (Rau *et al.*, 1982; Keller *et al.*, 2002). The decrease $\delta^{18}O_{shell}$ and $\delta^{13}C_{shell}$ with respect to the equilibrium was in agreement with the classical models driven by kinetic effects, that lead to isotope depleted carbonates (Adkins *et al.*, 2003), highlighting shell stable isotope vital effects in *C. gallina* and contributing to set limits for paleoenvironmental reconstructions for this species.

5. Conclusions

Bivalve shells can potentially provide information about past estuarine biogeochemical cycles by recording the carbon isotopic signature of dissolved inorganic carbon ($\delta^{13}C_{DIC}$) in estuarine waters. The Adriatic Sea, and especially its Northern basin, plays an important role in carbon cycling being a site of dense water formation during winter and one of the most productive areas in the Mediterranean, contributing to global biogeochemical cycling of carbon and nutrients (Crossland *et al.*, 2005; Catalano *et al.*, 2014). Here we present, for the first time, measurements of shell $\delta^{18}O$ and $\delta^{13}C$ of *C. gallina* combined with seawater $\delta^{18}O$ and $\delta^{13}C_{DIC}$ along the 400 km Western Adriatic coasts. The high variability of seawater parameters was expressed in the stable isotopic signature of *C. gallina* along the latitudinal gradient. *Chamelea gallina* from Northern sites clearly reflected lower temperature of deposition and the influence of Po river, while shells from Southern sites reflected the salty marine ingressions from the Southern Adriatic. Shells displayed depleted $\delta^{13}C$ values with decreasing salinity and increasing chlorophyll concentration, likely as a result of decreased calcification rates likely due to

increased eutrophication and silt and clay of the bottom driven by the river discharges. Almost all specimens exhibited depleted shell $\delta^{18}O$ and $\delta^{13}C$ values compared to the expected isotopic equilibrium. Hence, despite *C. gallina* showing promise as a warm temperature proxy, the large variation in the shell stable isotopic signature points toward noteworthy metabolic and/or kinetic effects in this bivalve, preventing the use of *C. gallina* as a paleoproxy for seawater temperatures.

REFERENCES

Adkins JF, Boyle EA, Curry WB, Lutringer A (2003) Stable isotopes in deep-sea corals and a new mechanism for "vital effects." *Geochimica et Cosmochimica Acta* **67**, 1129–1143.

Amorosi A, Barbieri G, Bruno L, Campo B, Drexler TM, Hong W, Rossi V, Sammartino I, Scarponi D, Vaiani SC, Bohacs KM (2019) Three-fold nature of coastal progradation during the Holocene eustatic highstand, Po Plain, Italy – close correspondence of stratal character with distribution patterns. *Sedimentology* **66**, 3029–3052.

Bargione G, Vasapollo C, Donato F, Virgili M, Petetta A, Lucchetti A (2020) Age and growth of Striped Venus Clam *Chamelea gallina* (Linnaeus, 1758) in the Mid-Western Adriatic Sea: A comparison of three laboratory techniques. *Frontiers in Marine Science* **7**, 807.

Bemis BE, Geary DH (1996) The usefulness of bivalve stable isotope profiles as environmental indicators: data from the Eastern Pacific Ocean and the Southern Caribbean Sea. *PALAIOS* **11**, 328.

Bemis BE, Spero HJ, Bijma J, Lea DW (1998) Reevaluation of the oxygen isotopic composition of planktonic foraminifera: Experimental results and revised paleotemperature equations. *Paleoceanography* **13**, 150–160.

Böhm F, Joachimski MM, Dullo W-C, Eisenhauer A, Lehnert H, Reitner J, Wörheide G (2000) Oxygen isotope fractionation in marine aragonite of coralline sponges. *Geochimica et Cosmochimica Acta* **64**, 1695–1703.

Bortolami G, Fontes J-CC, Panichi C (1973) Isotopes du milieu et circulations dans les aquiferes du sous-sol Vénitien. *Earth and Planetary Science Letters* **19**, 154–167.

Canuel EA, Cammer SS, McIntosh HA, Pondell CR (2012) Climate Change Impacts on the Organic Carbon Cycle at the Land-Ocean Interface. *Annual Review of Earth and Planetary Sciences* **40**, 685–711.

Catalano G, Azzaro M, Bastianini M, Bellucci LG, Bernardi Aubry F, Bianchi F, Burca M, Cantoni C, Caruso G, Casotti R, Cozzi S, Negro P Del, Fonda Umani S, Giani M, Giuliani S, Kovacevic V, Ferla R La, Langone L, Luchetta A, Monticelli LS, Piacentino S, Pugnetti A, Ravaioli M, Socal G, Spagnoli F, Ursella L (2014) The carbon budget in the northern Adriatic Sea, a winter case study. *Journal of Geophysical Research: Biogeosciences* **119**, 1399–1417.

Cespuglio G, Piccinetti C, Longinelli A (1999) Oxygen and carbon isotope profiles from *Nassa mutabilis* shells (Gastropoda): accretion rates and biological behaviour. *Marine Biology* **135**, 627–634.

Chauvaud L, Lorrain A, Dunbar RB, Paulet Y-M, Thouzeau G, Jean F, Guarini J-M, Mucciarone D (2005) Shell of the Great Scallop *Pecten maximus* as a high-frequency archive of paleoenvironmental changes. *Geochemistry, Geophysics, Geosystems* **6**.

Cheli A, Mancuso A, Azzarone M, Fermani S, Kaandorp J, Marin F, Montroni D, Polishchuk I, Prada F, Stagioni M (2021) Climate variation during the Holocene influenced the skeletal properties of *Chamelea gallina* shells in the North Adriatic Sea (Italy). *Plos one* **16**, e0247590.

Clarke A (1993) Temperature and extinction in the sea: a physiologist's view. *Paleobiology* **19**, 499–518.

Craig H (1965) The measurement of oxygen isotope paleotemperatures. *Stable isotopes in oceanographic studies and paleotemperatures: Consiglio Nazionale delle Richerche* 161–182.

Crossland CJ, Kremer HH, Lindeboom H, Crossland JIM, Tissier MDA Le (2005) *Coastal fluxes in the Anthropocene: the land-ocean interactions in the coastal zone project of the International Geosphere-Biosphere Programme*. Springer Science & Business Media.

Degobbis D, Gilmartin M, Revelante N (1986) An annotated nitrogen budget calculation for the northern Adriatic Sea. *Marine Chemistry* **20**, 159–177.

Elliot M, DeMenocal PB, Linsley BK, Howe SS (2003) Environmental controls on the stable isotopic composition of *Mercenaria mercenaria*: Potential application to paleoenvironmental studies. *Geochemistry, Geophysics, Geosystems* **4**.

Epstein S, Buchsbaum R, Lowenstam H, Urey HC (1951) Carbonate-water isotopic temperature scale. *Geological Society of America Bulletin* **62**, 417–426.

Epstein S, Mayeda T (1953) Variation of O^{18} content of waters from natural sources. *Geochimica et Cosmochimica Acta* **4**, 213–224.

Feely RA, Sabine CL, Lee K, Berelson W, Kleypas J, Fabry VJ, Millero FJ (2004) Impact of Anthropogenic CO 2 on the CaCO 3 System in the Oceans. *Science* **305**, 362–366.

529 Flora O, Longinelli A (1989) Stable isotope hydrology of a classical karst area, Trieste, Italy. In:
530 *Isotope techniques in the study of the hydrology of fractured and fissured rocks*.

531 Gazeau F, Quiblier C, Jansen JM, Gattuso J-P, Middelburg JJ, Heip CHR (2007) Impact of
532 elevated CO 2 on shellfish calcification. *Geophysical Research Letters* **34**, L07603.

533 Geist J, Auerswald K, Boom A (2005) Stable carbon isotopes in freshwater mussel shells:
534 Environmental record or marker for metabolic activity? *Geochimica et Cosmochimica Acta* **69**,
535 2662–2664.

536 Gillikin DP, Lorrain A, Bouillon S, Willenz P, Dehairs F (2006) Stable carbon isotopic
537 composition of Mytilus edulis shells: relation to metabolism, salinity, δ^{13}CDIC and
538 phytoplankton. *Organic Geochemistry* **37**, 1371–1382.

539 Gillikin DP, Lorrain A, Meng L, Dehairs F (2007) A large metabolic carbon contribution to the
540 δ^{13}C record in marine aragonitic bivalve shells. *Geochimica et Cosmochimica Acta* **71**, 2936–
541 2946.

542 Gillikin DP, Ridder F De, Ulens H, Elskens M, Keppens E, Baeyens W, Dehairs F (2005)
543 Assessing the reproducibility and reliability of estuarine bivalve shells (*Saxidomus giganteus*)
544 for sea surface temperature reconstruction: implications for paleoclimate studies.
545 *Palaeogeography, Palaeoclimatology, Palaeoecology* **228**, 70–85.

546 Gilmartin M, Degobbis D, Revelante N, Smodlaka N (1990) The mechanism controlling plant
547 nutrient concentrations in the northern Adriatic Sea. *Internationale Revue der gesamten*
548 *Hydrobiologie und Hydrographie* **75**, 425–445.

549 Giordani P, Helder W, Koning E, Miserocchi S, Danovaro R, Malaguti A (2002) Gradients of
550 benthic–pelagic coupling and carbon budgets in the Adriatic and Northern Ionian Sea. *Journal*
551 *of Marine Systems* **33**, 365–387.

552 Gizzi F, Caccia MG, Simoncini GA, Mancuso A, Reggi M, Fermani S, Brizi L, Fantazzini P,
553 Stagioni M, Falini G, Piccinetti C, Goffredo S (2016) Shell properties of commercial clam
554 Chamelea gallina are influenced by temperature and solar radiation along a wide latitudinal
555 gradient. *Scientific Reports* **6**, 36420.

556 Goodwin DH, Flessa KW, Schone BR, Dettman DL (2001) Cross-calibration of daily growth
557 increments, stable isotope variation, and temperature in the Gulf of California bivalve mollusk

Chione cortezi: implications for paleoenvironmental analysis. *PALAIOS* **16**, 387–398.

Goodwin DH, Schone BR, Dwttman DL (2003) Resolution and fidelity of oxygen isotopes as paleotemperature proxies in bivalve mollusk shells: models and observations. *PALAIOS* **18**, 110–125.

Grossman EL, Ku T-LL (1986) Oxygen and carbon isotope fractionation in biogenic aragonite: Temperature effects **59**, 59–74.

Hall-Spencer JM, Harvey BP (2019) Ocean acidification impacts on coastal ecosystem services due to habitat degradation. *Emerging Topics in Life Sciences* **3**, 197–206.

Harris KE, DeGrandpre MD, Hales B (2013) Aragonite saturation state dynamics in a coastal upwelling zone. *Geophysical Research Letters* **40**, 2720–2725.

Hickson JA, Johnson AL., Heaton TH., Balson PS (1999) The shell of the Queen Scallop *Aequipecten opercularis* (L.) as a promising tool for palaeoenvironmental reconstruction: Evidence and reasons for equilibrium stable-isotope incorporation. *Palaeogeography, Palaeoclimatology, Palaeoecology* **154**, 325–337.

Jones PD, Briffa KR, Osborn TJ, Lough JM, Ommen TD van, Vinther BM, Luterbacher J, Wahl ER, Zwiers FW, Mann ME, Schmidt GA, Ammann CM, Buckley BM, Cobb KM, Esper J, Goosse H, Graham N, Jansen E, Kiefer T, Kull C, Küttel M, Mosley-Thompson E, Overpeck JT, Riedwyl N, Schulz M, Tudhope AW, Villalba R, Wanner H, Wolff E, Xoplaki E (2009) High-resolution palaeoclimatology of the last millennium: a review of current status and future prospects. *The Holocene* **19**, 3–49.

Keller N, Piero D Del, Longinelli A (2002) Isotopic composition, growth rates and biological behaviour of *Chamelea gallina* and *Callista chione* from the Gulf of Trieste (Italy). *Marine Biology* **140**, 9–15.

Klein RT, Lohmann KC, Thayer CW (1996a) Bivalve skeletons record sea-surface temperature and $\delta^{18}O$ via Mg/Ca and $^{18}O/^{16}O$ ratios. *Geology* **24**, 415–418.

Klein RT, Lohmann KC, Thayer CW (1996b) Sr Ca and $^{13}C^{12}C$ ratios in skeletal calcite of Mytilus trossulus: Covariation with metabolic rate, salinity, and carbon isotopic composition of seawater. *Geochimica et Cosmochimica Acta* **60**, 4207–4221.

586 Krantz DE, Williams DF, Jones DS (1987) Ecological and paleoenvironmental information
587 using stable isotope profiles from living and fossil molluscs. *Palaeogeography,*
588 *Palaeoclimatology, Palaeoecology* **58**, 249–266.

589 Kubota K, Shirai K, Murakami-Sugihara N, Seike K, Hori M, Tanabe K (2017) Annual shell
590 growth pattern of the Stimpson's hard clam *Mercenaria stimpsoni* as revealed by
591 sclerochronological and oxygen stable isotope measurements. *Palaeogeography,*
592 *Palaeoclimatology, Palaeoecology* **465**, 307–315.

593 Leng MJ, Lewis JP (2016) Oxygen isotopes in Molluscan shell: Applications in environmental
594 archaeology. *Environmental Archaeology* **21**, 295–306.

595 Lorrain A, Paulet Y-M, Chauvaud L, Dunbar R, Mucciarone D, Fontugne M (2004) $\delta^{13}C$
596 variation in scallop shells: Increasing metabolic carbon contribution with body size?
597 *Geochimica et Cosmochimica Acta* **68**, 3509–3519.

598 Mancuso A, Stagioni M, Prada F, Scarponi D, Piccinetti C, Goffredo S (2019) Environmental
599 influence on calcification of the bivalve *Chamelea gallina* along a latitudinal gradient in the
600 Adriatic Sea. *Scientific Reports* **9**, 11198.

601 Marchina C (2015) Geochemical and isotopic investigation on the Po river waters from
602 Monviso sources to its delta: natural and anthropogenic components. *Unpublished Ph.D. thesis,*
603 *University of Ferrara*.

604 Matozzo V, Monari M, Foschi J, Serrazanetti GP, Cattani O, Marin MG (2007) Effects of salinity
605 on the clam *Chamelea gallina*. Part I: alterations in immune responses. *Marine Biology* **151**,
606 1051–1058.

607 McConnaughey T (1989a) ^{13}C and ^{18}O isotopic disequilibrium in biological carbonates: II. In
608 vitro simulation of kinetic isotope effects. *Geochimica et Cosmochimica Acta* **53**, 163–171.

609 McConnaughey T (1989b) ^{13}C and ^{18}O isotopic disequilibrium in biological carbonates: I.
610 Patterns. *Geochimica et Cosmochimica Acta* **53**, 151–162.

611 McConnaughey TA, Burdett J, Whelan JF, Paull CK (1997) Carbon isotopes in biological
612 carbonates: Respiration and photosynthesis. *Geochimica et Cosmochimica Acta* **61**, 611–622.

613 McConnaughey TA, Gillikin DP (2008) Carbon isotopes in mollusk shell carbonates. *Geo-*

614 *Marine Letters* **28**, 287–299.

615 Monari M, Matozzo V, Foschi J, Cattani O, Serrazanetti GP, Marin MG (2007a) Effects of high
616 temperatures on functional responses of haemocytes in the clam *Chamelea gallina*. *Fish and*
617 *Shellfish Immunology*.

618 Monari M, Serrazanetti GP, Foschi J, Matozzo V, Marin MG, Cattani O (2007b) Effects of salinity
619 on the clam *Chamelea gallina* haemocytes. Part II: Superoxide dismutase response. *Marine*
620 *Biology*.

621 Montanari A (2012) Hydrology of the Po River: looking for changing patterns in river
622 discharge. *Hydrology and Earth System Sciences* **16**, 3739–3747.

623 Mook WG, Vogel JC (1968) Isotopic equilibrium between shells and their environment. *Science*
624 **159**, 874–875.

625 Peharda M, Vilibić I, Black B, Uvanović H, Markulin K, Mihanović H (2019) A network of
626 bivalve chronologies from semi-enclosed seas. *Plos one* **14**, e0220520.

627 Pérez CA, Lagos NA, Saldías GS, Waldbusser G, Vargas CA (2016) Riverine discharges impact
628 physiological traits and carbon sources for shell carbonate in the marine intertidal mussel
629 *Perumytilus purpuratus*. *Limnology and Oceanography* **61**, 969–983.

630 Pettine M, Patrolecco L, Camusso M, Crescenzio S (1998) Transport of carbon and nitrogen to
631 the northern Adriatic Sea by the Po River. *Estuarine, Coastal and Shelf Science* **46**, 127–142.

632 Pierre C (1999) The oxygen and carbon isotope distribution in the Mediterranean water
633 masses. *Marine Geology* **153**, 41–55.

634 Prada F, Yam R, Levy O, Caroselli E, Falini G, Dubinsky Z, Goffredo S, Shemesh A (2019) Kinetic
635 and metabolic isotope effects in zooxanthellate and non-zooxanthellate Mediterranean corals
636 along a wide latitudinal gradient. *Frontiers in Marine Science* **6**, 522.

637 Purroy A, Milano S, Schöne BR, Thébault J, Peharda M (2018) Drivers of shell growth of the
638 bivalve, *Callista chione* (L. 1758) – Combined environmental and biological factors. *Marine*
639 *Environmental Research* **134**, 138–149.

640 Raicich F (1996) On the fresh balance of the Adriatic Sea. *Journal of Marine Systems* **9**, 305–

641 319.

642 Rau GH, Sweeney RE, Kaplan IR (1982) Plankton ^{13}C:^{12}C ratio changes with latitude:
643 differences between northern and southern oceans. *Deep Sea Research Part A, Oceanographic*
644 *Research Papers*.

645 Regnier P, Friedlingstein P, Ciais P, Mackenzie FT, Gruber N, Janssens IA, Laruelle GG,
646 Lauerwald R, Luyssaert S, Andersson AJ, Arndt S, Arnosti C, Borges A V., Dale AW, Gallego-Sala
647 A, Goddéris Y, Goossens N, Hartmann J, Heinze C, Ilyina T, Joos F, LaRowe DE, Leifeld J,
648 Meysman FJR, Munhoven G, Raymond PA, Spahni R, Suntharalingam P, Thullner M (2013)
649 Anthropogenic perturbation of the carbon fluxes from land to ocean. *Nature Geoscience* **6**,
650 597–607.

651 Rhoads D, Lutz R (1980) Skeletal growth of aquatic organisms: biological records of
652 environmental change.

653 Richardson CA (2001) Molluscs as archives of environmental change.

654 Ridente D, Foglini F, Minisini D, Trincardi F, Verdicchio G (2007) Shelf-edge erosion, sediment
655 failure and inception of Bari Canyon on the Southwestern Adriatic Margin (Central
656 Mediterranean). *Marine Geology* **246**, 193–207.

657 Ridente D, Trincardi F, Piva A, Asioli A, Cattaneo A (2008) Sedimentary response to climate
658 and sea level changes during the past~ 400 ka from borehole PRAD1–2 (Adriatic margin).
659 *Geochemistry, Geophysics, Geosystems* **9**.

660 Romanek CS, Grossman EL, Morse JW (1992) Carbon isotopic fractionation in synthetic
661 aragonite and calcite: Effects of temperature and precipitation rate. *Geochimica et*
662 *Cosmochimica Acta* **56**, 419–430.

663 Rosenberg GD, Hughe WW (1991) A metabolic model for the determination of shell
664 composition in the bivalve mollusc, *Mytilus edulis*. *Lethaia* **24**, 83–96.

665 RStudio Team (2020) RStudio: Integrated Development for R. RStudio, PBC, Boston, MA URL
666 http://www.rstudio.com/.

667 Russo A, Artegiani A (1996) Adriatic sea hydrography. *Scientia Marina* **60**, 33–43.

668 Sadler J, Carré M, Azzoug M, Schauer AJ, Ledesma J, Cardenas F, Chase BM, Bentaleb I, Muller
669 SD, Mandeng M, Rohling EJ, Sachs JP (2012) Reconstructing past upwelling intensity and the
670 seasonal dynamics of primary productivity along the Peruvian coastline from mollusk shell
671 stable isotopes. *Geochemistry, Geophysics, Geosystems* **13**, n/a-n/a.

672 Salisbury J, Green M, Hunt C, Campbell J (2008) Coastal acidification by rivers: a threat to
673 shellfish? *Eos, Transactions American Geophysical Union* **89**, 513–513.

674 Schöne B, Tanabe K, Dettman D, Sato S (2003) Environmental controls on shell growth rates
675 and $\delta^{18}O$ of the shallow-marine bivalve mollusk *Phacosoma japonicum* in Japan. *Marine*
676 *Biology* **142**, 473–485.

677 Schöne BR (2008) The curse of physiology—challenges and opportunities in the
678 interpretation of geochemical data from mollusk shells. *Geo-Marine Letters* **28**, 269–285.

679 Schöne BR, Gillikin DP (2013) Unraveling environmental histories from skeletal diaries —
680 Advances in sclerochronology. *Palaeogeography, Palaeoclimatology, Palaeoecology* **373**, 1–5.

681 Spero HJ, Bijma J, Lea DW, Bemis BE (1997) Effect of seawater carbonate concentration on
682 foraminiferal carbon and oxygen isotopes. *Nature* **390**, 497–500.

683 Stenni B, Nichetto P, Bregant D, Scarazzato P, Longinelli A (1995) The Delta-O-18 signal of the
684 northward flow of mediterranean waters in the Adriatic Sea. *Oceanologica acta* **18**, 319–328.

685 Tanabe K, Oba T (1988) Latitudinal variation in shell growth patterns of *Phacosoma*
686 *japonicum* (Bivalvia: Veneridae) from the Japanese coast. *Marine Ecology Progress Series* 75–
687 82.

688 Tanaka N, Monaghan MC, Rye DM (1986) Contribution of metabolic carbon to mollusc and
689 barnacle shell carbonate. *Nature* **320**, 520–523.

690 Tesi T, Miserocchi S, Goni MA e a1, Langone L, Boldrin A, Turchetto M (2007) Organic matter
691 origin and distribution in suspended particulate materials and surficial sediments from the
692 western Adriatic Sea (Italy). *Estuarine, Coastal and Shelf Science* **73**, 431–446.

693 Tripati AK, Eagle RA, Thiagarajan N, Gagnon AC, Bauch H, Halloran PR, Eiler JM (2010) ^{13}C–^{18}O
694 isotope signatures and 'clumped isotope' thermometry in foraminifera and coccoliths.
695 *Geochimica et Cosmochimica Acta* **74**, 5697–5717.

696 Urey HC (1948) Oxygen Isotopes in Nature and in the Laboratory. *New Series* **108**, 489–496.

697 Uvanović H, Schöne BR, Markulin K, Janeković I, Peharda M (2021) Venerid bivalve *Venus*
698 *verrucosa* as a high-resolution archive of seawater temperature in the Mediterranean Sea.
699 *Palaeogeography, Palaeoclimatology, Palaeoecology* **561**, 110057.

700 Vihtakari M, Ambrose WG, Renaud PE, Locke WL, Carroll ML, Berge J, Clarke LJ, Cottier F, Hop
701 H (2017) A key to the past? Element ratios as environmental proxies in two Arctic bivalves.
702 *Palaeogeography, Palaeoclimatology, Palaeoecology* **465**, 316–332.

703 Wefer G, Berger WH (1991) Isotope paleontology: growth and composition of extant
704 calcareous species. *Marine Geology* **100**, 207–248.

705 Wheeler A (1992) Mechanisms of molluscan shell formation. *Calcification in Biological*
706 *Systems*.

707 Zavatarelli M, Raicich F, Bregant D, Russo A, Artegiani A (1998) Climatological biogeochemical
708 characteristics of the Adriatic Sea. *Journal of Marine Systems* **18**, 227–263.

709 Zeebe RE (1999) An explanation of the effect of seawater carbonate concentration on
710 foraminiferal oxygen isotopes. *Geochimica et Cosmochimica Acta* **63**, 2001–2007.

711

712 **TABLES**
713
714 **Table 1. Seawater Isotope data.** $\delta^{18}O_{sw}$ (summer, winter and annual average seawater) and
715 $\delta^{13}C_{DIC}$ (summer, winter and annual average seawater). Values for each site in decreasing
716 order of latitude: MO (Monfalcone), CH (Chioggia), GO (Goro), CE (Cesenatico), SB (San
717 Benedetto), CA (Capoiale). K-W, Kruskal-Wallis test; *** $p<0.001$.

Site	Latitude (°)	Summer $\delta^{18}O_{sw}$	Winter $\delta^{18}O_{sw}$	Annual mean $\delta^{18}O_{sw}$	Summer $\delta^{13}C_{DIC}$	Winter $\delta^{13}C_{DIC}$	Annual mean $\delta^{13}C_{DIC}$
MO	45.70	0.80	0.12	0.46	-0.05	-1.91	-0.98
CH	45.20	-1.24	0.87	-0.19	-0.73	-0.79	-0.76
GO	44.78	-2.84	-0.65	-1.75	-3.54	-2.34	-2.94
CE	44.18	0.47	-0.60	-0.06	-1.56	-1.88	-1.72
SB	43.08	1.32	0.68	1.00	-0.21	-0.79	-0.50
CA	41.92	1.63	1.41	1.52	0.28	0.11	0.20
K-W		***	***	***	***	***	***

718

719 **Table 2. Shell Isotope data**. SE, standard error of the shell isotope values for each site. KW,
720 Kruskal-Wallis test; *** $p<0.001$. Values for each site in decreasing order of latitude: MO
721 (Monfalcone), CH (Chioggia), GO (Goro), CE (Cesenatico), SB (San Benedetto), CA (Capoiale).

Site	n	$\delta^{18}O_{shell}$ (SE)	$\delta^{18}O_{shell}$ - $\delta^{18}O_{sw}$	$\delta^{13}C_{shell}$ (SE)	$\delta^{13}C_{shell}$ - $\delta^{13}C_{DIC}$
MO	8	-0.31 (0.12)	-0.76	-1.47 (0.11)	-0.49
CH	7	-0.83 (0.04)	-0.64	-1.16 (0.10)	-0.40
GO	7	-0.98 (0.20)	0.76	-2.14 (0.15)	0.80
CE	7	-0.91 (0.16)	-0.85	-1.62 (0.11)	0.10
SB	7	-0.08 (0.11)	-1.08	-1.20 (0.09)	-0.69
CA	7	0.24 (0.08)	-1.28	-0.34 (0.05)	-0.54
K-W		***	***	***	***

722
723
724
725

726 **FIGURES LEGEND**

727

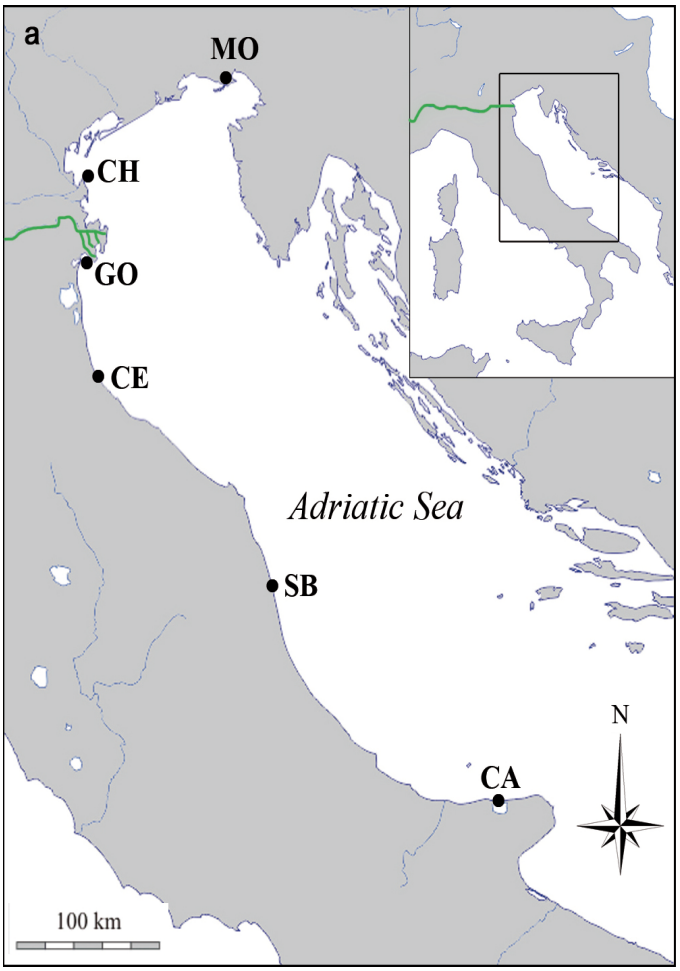

b

Site	Code	Latitude (°)
Monfalcone	MO	45.7
Chioggia	CH	45.2
Goro	GO	44.8
Cesenatico	CE	44.2
San Benedetto	SB	43.1
Capoiale	CA	41.9

c

Code	n	SST (°C) mean (SE)	SSS (PSU) mean (SE)
MO	1447	16.96 (0.19)	35.43 (0.03)
CH	1447	16.47 (0.19)	30.89 (0.09)
GO	1447	16.54 (0.19)	28.52 (0.08)
CE	1447	17.05 (0.20)	34.19 (0.04)
SB	1447	17.90 (0.19)	36.29 (0.03)
CA	1447	18.60 (0.17)	37.43 (0.01)

d

Code	n	CHL (mg/m^3) mean (SE)
MO	48	4.5 (0.20)
CH	48	2.88 (0.22)
GO	48	4.98 (0.38)
CE	48	6.23 (0.59)
SB	48	2.09 (0.27)
CA	48	1.21 (0.18)

Figure 1. Map of the Adriatic Sea and environmental parameters.

a. Adriatic coastline with sampling sites of C. gallina clams. Po river labelled with green lines. Abbreviations and coordinates of the sites in decreasing order of latitude: MO, Monfalcone 45°42'N, 13°14'E; CH, Chioggia 45°12'N, 12°19'E; GO, Goro 44°47'N, 12°25'E; CE, Cesenatico 44°11'N, 12°26'E; SB, San Benedetto 43°5'N, 13°51'E; CA, Capoiale 41°55'N, 15°39'E. The map was downloaded from d-maps.com site (http://www.d-maps.com) and modified with Adobe Photoshop CS4. b-c-d. Latitude, annual average values for sea surface temperature (SST), sea surface salinity (SSS) and chlorophyll concentration (CHL) from 2011 to 2015. n = number of collected data, daily data for SST and SSS and monthly data for CHL; SE = standard error.

728

729
730
731

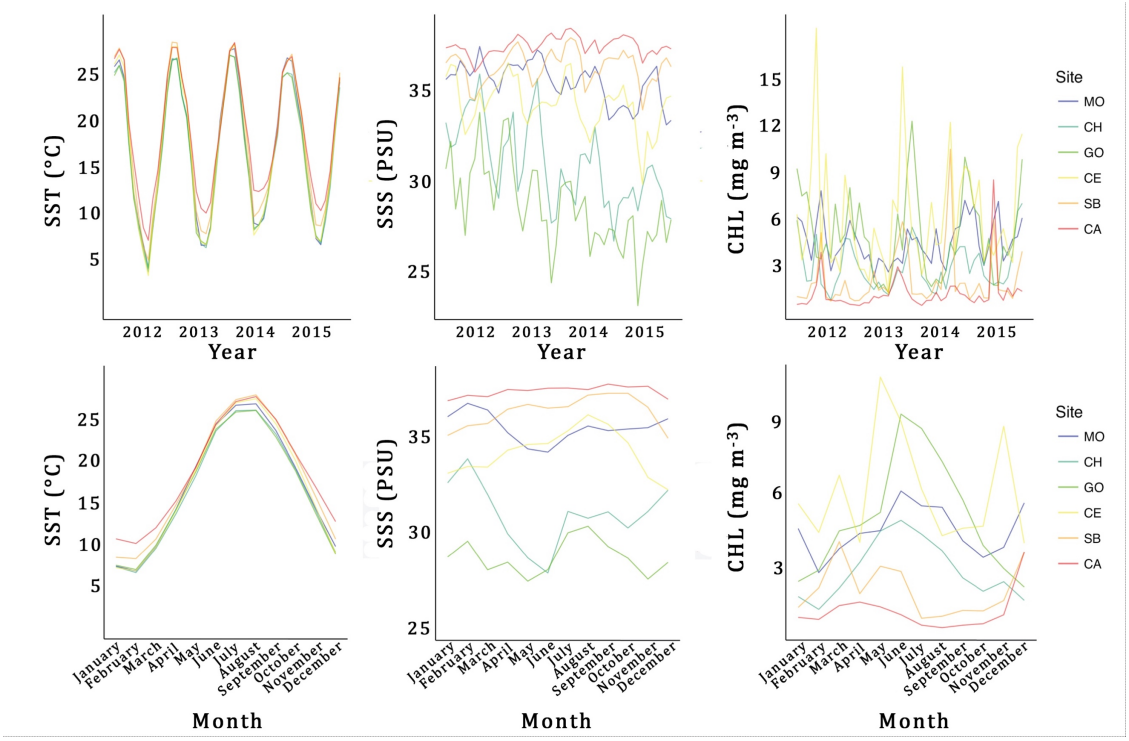

Figure 2. Inter-annual and intra-annual variations of SST, SSS and CHL among sites. Inter-annual data from July 2011 to June 2015. Intra-annual data are the mean monthly values of four years. Abbreviations in decreasing order of latitude: MO, Monfalcone; CH, Chioggia; GO, Goro; CE, Cesenatico; SB, San Benedetto; CA, Capoiale.

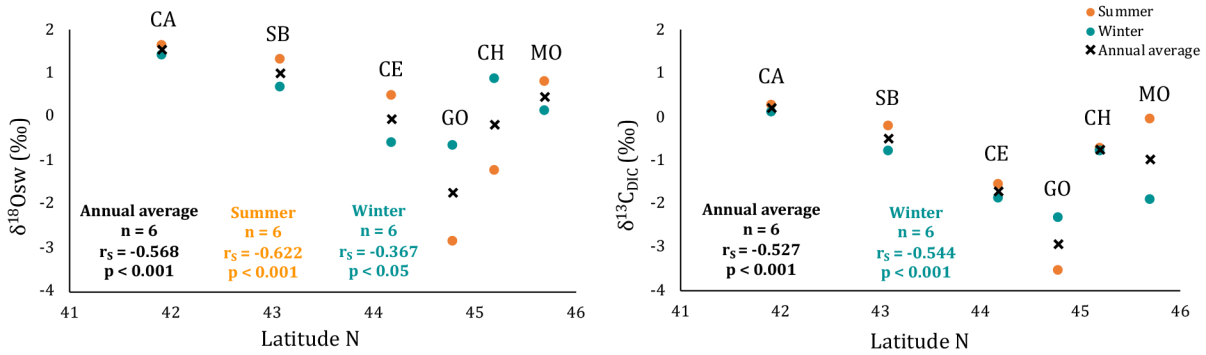

Figure 3. The relation between summer, winter and annual mean $\delta^{18}O_{sw}$ and $\delta^{13}C_{DIC}$ with latitude in six sites along the Western coast of the Adriatic Sea (~400 km transect). Orange dots are summer values, green dots are the winter ones and black crosses are the annual isotope average between summer and winter. No statistics included for summer $\delta^{13}C_{DIC}$ because of lack of statistically significant. MO, Monfalcone; CH, Chioggia; GO, Goro; CE, Cesenatico; SB, San Benedetto; CA, Capoiale.

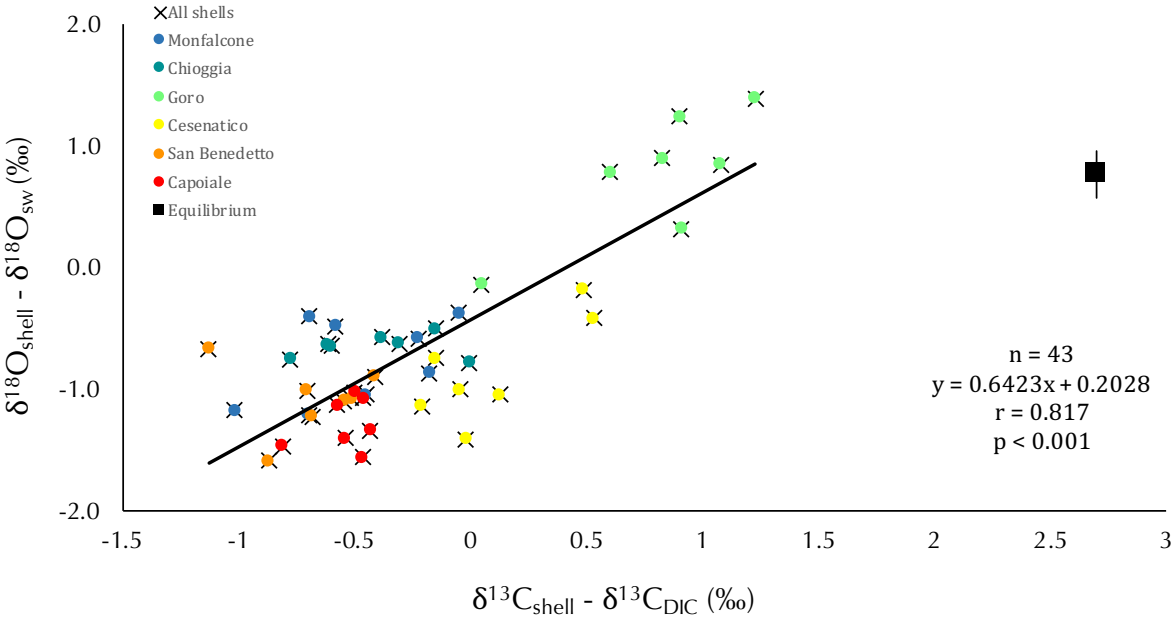

Figure 4. Isotopic comparison among the six sites along the Adriatic coasts of Italy. The black square depicts the mean estimated aragonite equilibrium value among sites, and the

745 vertical line shows the range of equilibrium values related to local maximum and minimum
746 temperature along the gradient.

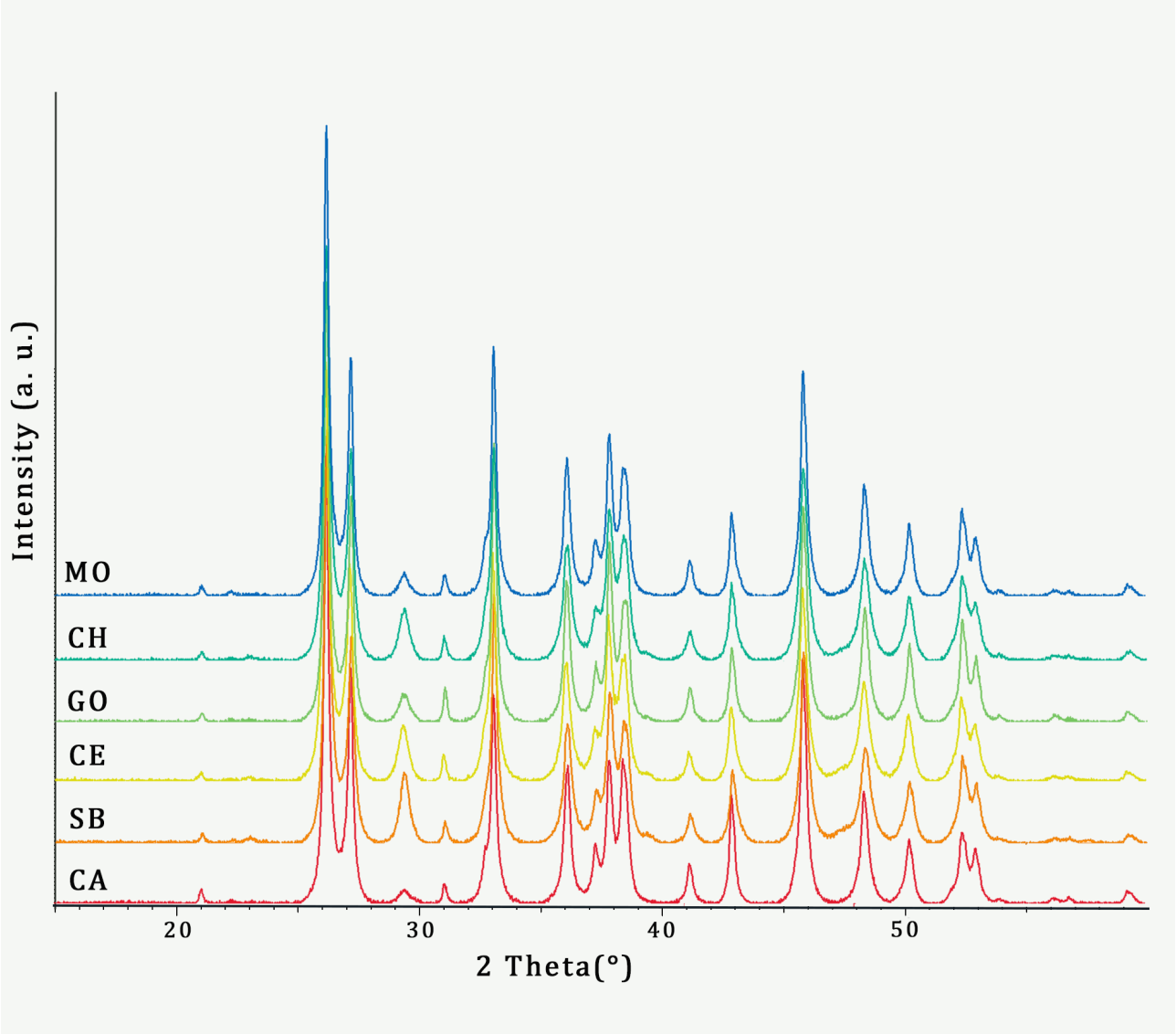

747

748 **Figure 5. X-ray powder diffraction (XRD) patterns from ground shells of *C. gallina*.** A
749 diffraction pattern is shown for each site. All the peaks were assigned to aragonite.

750

751

752

753

754

755

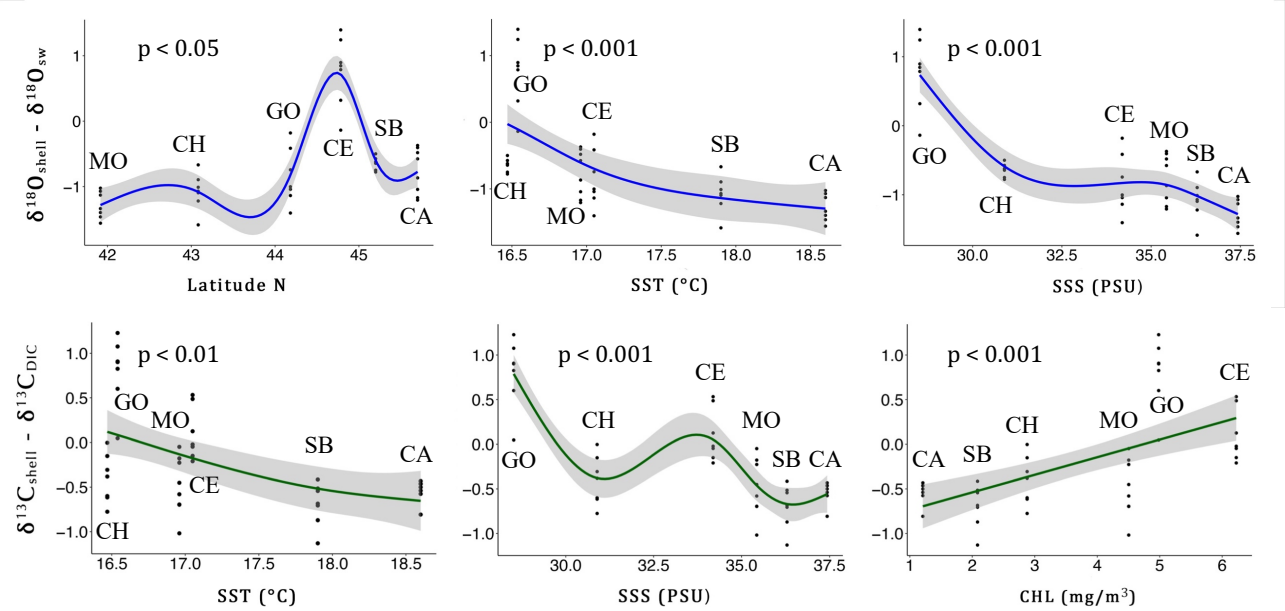

Figure 6. Estimated smooth curve from GAM models. Scatterplots of $\delta^{18}O_{shell}$ - $\delta^{18}O_{sw}$ and $\delta^{13}C_{shell}$ - $\delta^{13}C_{DIC}$ with fitted smooth terms s(Lat), s(SST), s(SSS), s(CHL) (solid line). Number of degrees of freedom=*6* and 95% confidence intervals (grey shade). See Table 3 for statistics.

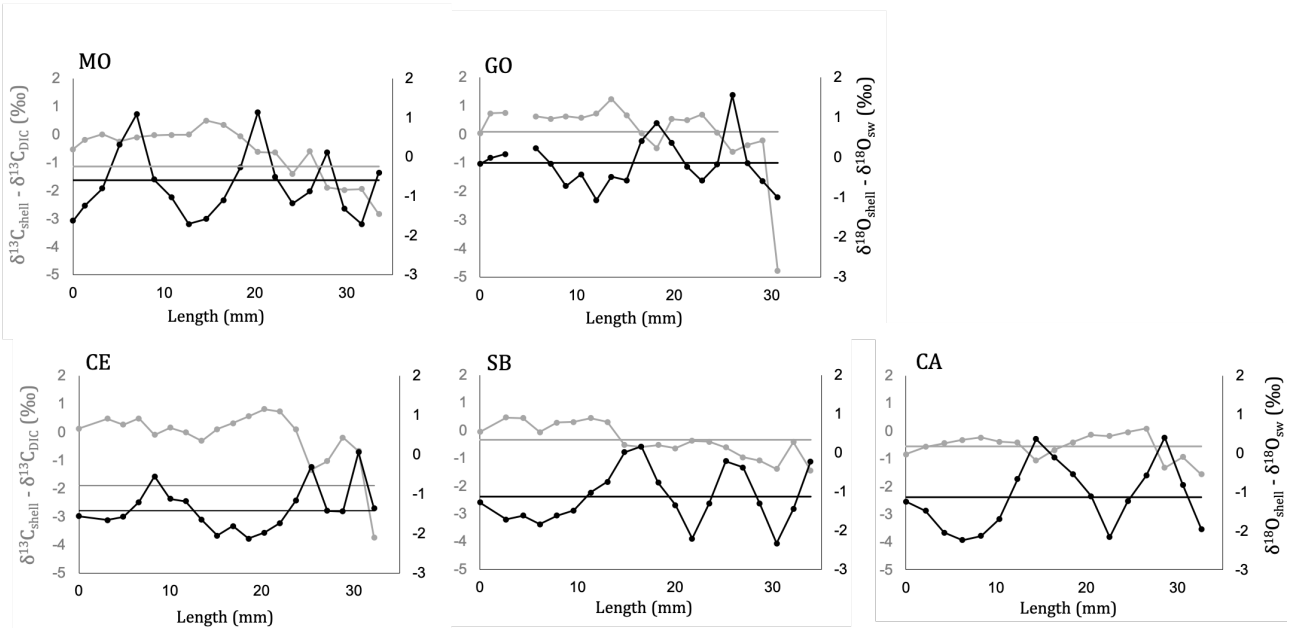

762

763 **Figure 7. $\delta^{18}O_{shell}$ - $\delta^{18}O_{sw}$ and $\delta^{13}C_{shell}$ - $\delta^{13}C_{DIC}$ profiles along the shell growth axis**. Grey

764 lines represent $\delta^{13}C$, black lines are $\delta^{18}O$ and points on the lines are the drilled spots. The lower

765 values indicate summer, while the higher values indicate winter. The average values of the

766 drilled spots at each site are reported as horizontal line. No seasonal data for Chioggia.

767

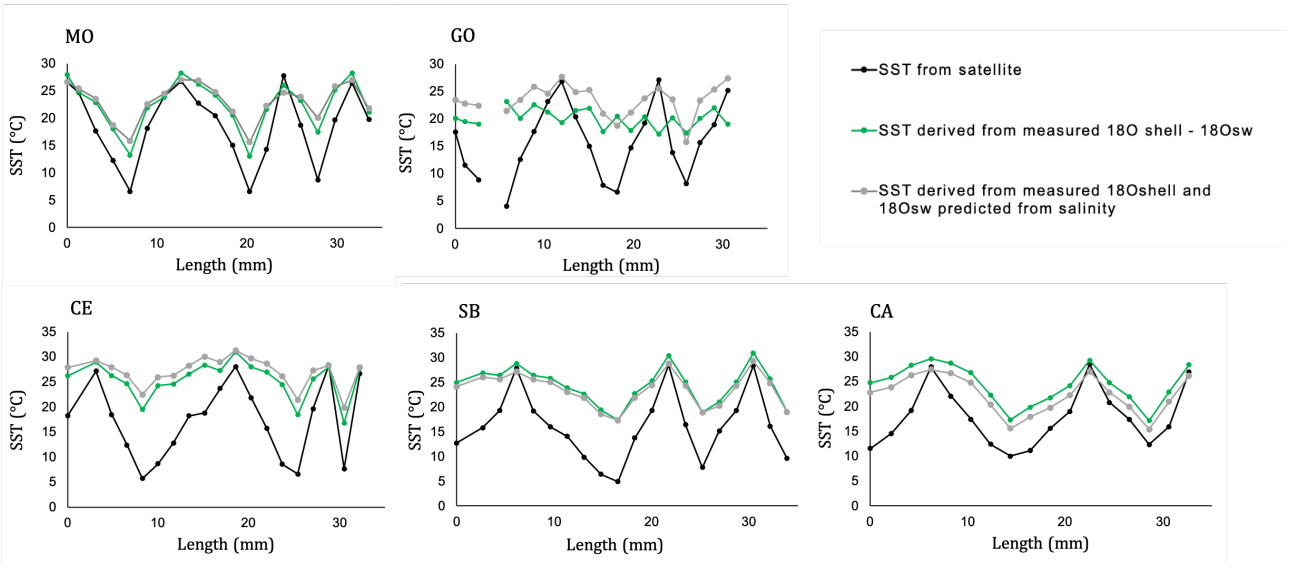

768

769 **Figure 8. Comparison between SST from satellite and derived SST from oxygen isotopes**

770 **of *C. gallina*.** SST derived from $\delta^{18}O_{shell}$ along shell growth axis and measured $\delta^{18}O_{sw}$ (green

771 line) and predicted $\delta^{18}O_{sw}$ (grey line), using the equation from Grossman and Ku,

772 1986(Grossman & Ku, 1986) [T = 20.6 – 4.34($\delta^{18}O_{arag}$ – ($\delta^{18}O_{sw}$ - 0.27))]. Winter, summer or
773 average $\delta^{18}O_{sw}$ were considered depending on seasonal profile observed in the sinusoidal
774 sequence of oxygen isotopes during shell growth. Predicted $\delta^{18}O_{sw}$ was calculated from salinity
775 data (grey line) using the equation derived from Purroy *et al.*, 2018 [$\delta^{18}O_{sw}$ = 0.23 x salinity -
776 7.54]. Winter, summer or average salinity SST obtained from satellite data (balck line).
777

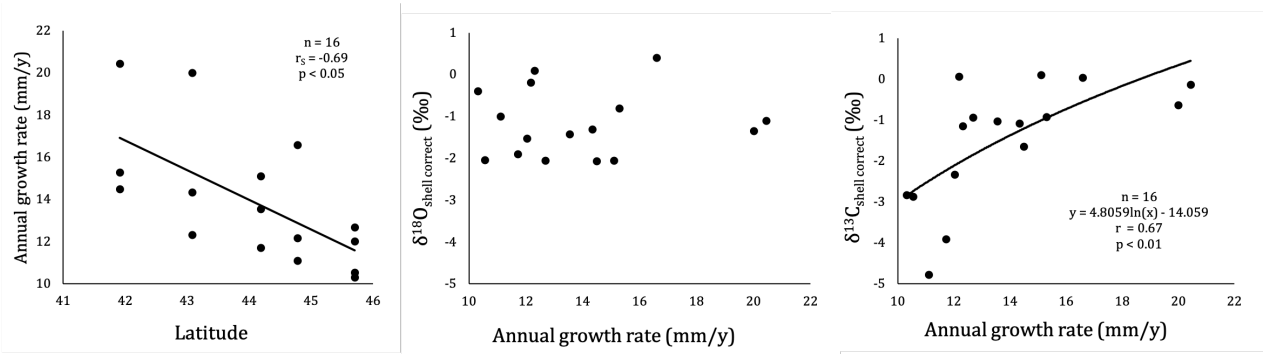

778 **Figure 9. Relationship between annual growth rates with latitude, $\delta^{18}O_{shell}$ - $\delta^{18}O_{sw}$ and**
779 **$\delta^{13}C_{shell}$ - $\delta^{13}C_{DIC}$.** Growth rates are calculated from the length-age key at each year, by means of
780 $\delta^{18}O$ profile along the shell growth axis.
781
782
783